Snap-Off of a Liquid Drop Immersed in Another Liquid Flowing Through a Constricted Capillary

T. J. Peña and M. S. Carvalho
PUC-Rio, Dept. of Mechanical Engineering, Rua Marquês de São Vicente, 225 Gávea, Rio de Janeiro, RJ, Brazil, 22453-900

V. Alvarado
University of Wyoming, Dept. of Chemical and Petroleum Engineering, Dept. 3295, 1000 E. University Avenue, Laramie, WY 82071

DOI 10.1002/aic.11839
Published online June 23, 2009 in Wiley InterScience (www.interscience.wiley.com).

Emulsions are encountered at different stages of oil production processes, often impacting many aspects of oilfield operations. Emulsions may form as oil and water come in contact inside the reservoir rock, valves, pumps, and other equipments. Snap-off is a possible mechanism to explain emulsion formation in two-phase flow in porous media. Quartz capillary tubes with a constriction (pore neck) served to analyze snap-off of long (''infinite'') oil droplets as a function of capillary number and oil-water viscosity ratio. The flow of large oil drops through the constriction and the drop breakup process were visualized using an optical microscope. Snap-off occurrence was mapped as a function of flow parameters. High oil viscosity suppresses the breakup process, whereas snap-up was always observed at low dispersed-phase viscosity. At moderate viscosity oil/water ratio, snap-off was observed only at low capillary number. Mechanistic explanations based on competing forces in the liquid phases were proposed. © 2009 American Institute of Chemical Engineers *AIChE J,* 55: 1993–1999, 2009
Keywords: emulsions, capillary model, snap-off, dispersions, porous media

Introduction

Emulsions are systems where at least one liquid phase is dispersed in a second liquid, continuous phase. Emulsions are generally stabilized by addition of a surfactant, which acts by reducing the interfacial tension between the two liquid phases involved, and by creating repulsive (steric) forces between droplets, to limit coalescence. Emulsions are frequently encountered in industrial processes such as in adhesive coatings, inks, foods, cosmetics, controlled dosage medicines, and in practically all the stages of oil production.

Emulsions can be produced spontaneously or in controlled ways. Controlled emulsion production involves shear and extensional flows to cause enough deformation of drops to cause breakup, such as in mixers or homogenizers, or physico–chemical processes, separately or combined. Recent interest has sparked from drug-delivery applications.[1] Mixers produce highly poly-disperse emulsions, which are not appropriate for drug delivery applications. An alternative method is provided by membrane technologies, which improve emulsification conditions by using narrow pore-size distributions in membrane supports.[1] It has been shown that the mean drop size depends strongly on the mean pore size in the membrane.[1] Interesting applications include water in oil in water emulsions (W/O/W) for anticancer drug delivery.[1] Double emulsions in multiple-phase systems has also been produced.[2] The role of dynamic interfacial tension has been discussed by van der Graaf et al.[3]

The upsurge of microfluidics technologies provides the highest potential for generation of highly monodisperse emulsions.[4,5] Droplet microfluidics arises as a powerful

Correspondence concerning this article should be addressed to V. Alvarado at valvarad@uwyo.edu or vladimir@yahoo.com
Current address of T. J. Peña: Alberta Research Council, Heavy Oil and Oil Sands, 250 Karl Clark Road, Edmonton, Alberta, Canada, T6N 1E4

option to perform a large number of reactions without increasing device size or complexity.[6] Microfulidics devices offer control of local flow by fabrication of complex microscale geometries. Passive methods for forming droplets usually fall in three categories, in terms of the nature of the flow field near the pinchoff: (1) Co-flowing streams, (2) Cross-flowing streams (T-junctions), and (3) Elongation-dominated flows.[4] A competition between the local fluid stresses acting to deform the interface and capillary pressure resisting the deformation defines the break up mechanism and drop size. In flow focusing devices, two immiscible liquids flow coaxially into separate channels in a planar geometry. Downstream, the two liquids meet at the tip of the inner microchannel. Two regimes of drop production have been identified: dripping and jetting.[4] Recent attempts to increase droplet productivity in microfluidic devices have been carried out with integrated quadra-droplet generators.[7]

In oil production, emulsions are formed spontaneously as oil and water of certain composition enter in contact. Emulsion formation in oil production may take place inside the reservoir, in the two-phase flow in production wells and in the flow through pipes and valves. According to Davies, Nilsen, and Gramme,[8] and Sarbar and Wingrove,[9] emulsions formed spontaneously in oil production may be stabilized by some components of the oil, typically heavy oil fractions, and suspended solids. Most crude oil in the World is in fact produced as water-in-oil (more commonly) or oil-in-water (generally at high watercut) emulsions.

Uncontrolled emulsion formation during oil production leads to many operational problems and increase in operating cost, due to frequent equipment shut-down for maintenance and the unexpected need for large separation equipments. The produced emulsions have to be treated to remove the water and associated inorganic salts to meet crude oil specification for transportation and storage and to reduce corrosion in downstream process facilities. Kokal[10] classified oil-water emulsions based on the time required for phase separation in loose emulsion, which takes only a few minutes for separation to occur, medium and tight emulsions, for which phases separate partially only after days. The residence time required in separation equipments is a direct function of the size of the drops of the dispersed phase and the density difference between the phases. The morphology of the produced emulsion strongly affects the flow characteristics in wells, risers (in offshore production), equipments, and pipelines. This morphology changes as the operating conditions of an oil field evolve in time, changing in turn the flow rate-pressure drop relationship for emulsion flow. Therefore, understanding of the emulsification processes that occur during oil production and the morphology of the resulting emulsion is vital in the design of different equipment and in production optimization.

Emulsion formation starts inside the oil reservoir as a result of the flow of two immiscible liquids (water and oil) through a complex interconnected pore-neck system. The characteristics of the oil-water mixtures flowing in a porous media were examined by Jensen[11] with core-flow and micromodel experiments. They measured the drop size distribution at different flow conditions. The nonwetting phase may become disconnected leading to the formation of small drops by different mechanisms. One of these mechanisms is the so-called snap-off, which may be described as the invasion

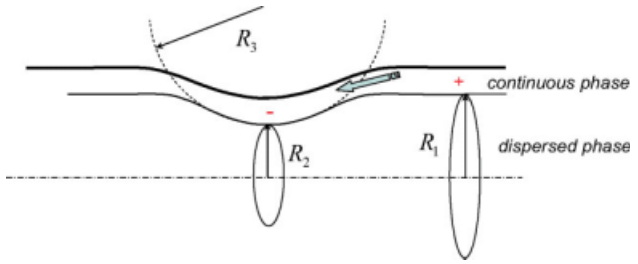

Figure 1. Sketch of interface configuration near the capillary throat.

[Color figure can be viewed in the online issue, which is available at www.interscience.wiley.com.]

of the wetting phase flowing adjacent to the pore-neck wall into a constriction occupied mostly by a non-wetting phase. The wetting film grows like a collar until it creates a discontinuity in the nonwetting phase. Roof[12] analyzed with a simple quasi-static model and experimental visualization the flow of an oil drop through a doughnut hole constriction into a water-filled pore. He considered the pressure to be constant inside the drop. Because of the higher curvature of the interface in the throat, the pressure in the continuous phase is smaller there, creating a capillary pressure difference that drives the liquid toward the constriction, as sketched in Figure 1. Roof developed a criterion based on the geometry of the constriction that defines the occurrence of snap-off. The same type of break-up was observed experimentally by Olbricht and Leal,[13] and Aul and Olbricht.[14]

For nonstatic conditions, snap-off occurs if the time a collar of the continuous phase takes to grow until breakup is smaller than the residence time of the drop in the constriction. Tsai and Miksis[15] showed by numerical simulation that snap-off occurs for a limited range of capillary number. Below a critical value, the film thickness of the continuous phase attached to the wall is very thin and the flow rate towards the constriction very low, leading to extremely long snap-off time. Above a second critical value, the residence time of the drop becomes so small that the water collar cannot develop. Experimental results presented by Arriola, Willhite, and Green[16] show that the snap-off process in noncircular throats is much faster than in cylindrical constricted capillaries. The corners of the channel reduce the flow resistance towards the throat, leading to much higher flow rates of the continuous phase. Ratulowski and Chang[17] analyzed theoretically the breakup in constricted capillaries with circular and square cross sections.

The snap-off process is also the main mechanism for foam generation inside a porous media. Gauglitz, Laurent, and Radke[18] studied the snap-off of large bubbles as they moved through a smooth cylindrical constriction. They measured the break-up time as a function of the capillary number. A theoretical model to study the dynamics of a wetting liquid film forming an unstable collar in a constricted capillary was developed by Gauglitz and Radke.[19]

The flow rate of the continuous phase toward the capillary throat through the thin film attached to the wall and consequently the snap off time is determined by three competing forces: the capillary pressure difference that drives the

continuous phase towards the constriction, the flow resistance of the wetting liquid, and the squeezing process of the discrete phase. The last force is usually ignored in most analyses, although it has been observed that snap-off does not occur if the drop viscosity is much larger than the wetting liquid, even when the snap-off criterion of Roof's[12] was satisfied (see[20]).

Here, we study the snap-off of large ("infinite") liquid drops immersed in a continuous liquid as they flow through a cylindrical constriction. A simple model to estimate the effect of the drop viscosity on the continuous phase flow rate, and consequently on the snap-off time, is presented. Experiments with a transparent constricted capillary and different liquid systems, covering a wide range of viscosity ratio, were performed to map the region of the flow parameter space at which snap-off occurs.

Effect of Viscosity Ratio on the Snap-Off Mechanism

As described by Roof,[12] the pressure difference that drives liquid towards the capillary constriction emerges from the curvature difference of the interface, that is,

$$P_{L1} - P_{L2} = \sigma\left(\frac{1}{R_2} - \frac{1}{R_1} - \frac{1}{R_3}\right); \tag{1}$$

As indicated in Fig. 1, R_1 and R_2 are the circumferential radii of curvature of the interface away from (point 1) and at (point 2) the capillary throat; and R_3 is the transversal radius of curvature of the interface at the constriction. In the case of snap-off of gas bubbles, the only force that opposes this flow is the viscous stress at the capillary wall, proportional to the liquid viscosity and inversely proportional to the thickness of the film. Because of the low viscosity of the gas, the shear stress at the interface and the pressure drop on the gas bubble are neglected.

In the case of snap-off of a viscous drop, the squeezing process of the drop as the collar grows and the shear stress at the interface between the two liquids represent extra forces that act against the capillary driven flow that causes snap-off. The effect of the dispersed phase viscosity can be estimated by analyzing the two-phase rectilinear flow away from the constriction, as indicated in Figure 2. As the continuous phase flows towards the constriction, the dispersed phase has to flow away from it; the pressure difference on both phases have opposite signs and are related by the capillary pressure difference:

$$\underbrace{P_{C1} - P_{C2}}_{>0} = \underbrace{P_{D1} - P_{D2}}_{<0} + \underbrace{\sigma\left(\frac{1}{R_2} - \frac{1}{R_1} - \frac{1}{R_3}\right)}_{>0}; \tag{2}$$

$$\Delta P_C = \Delta P_D + \sigma\left(\frac{1}{R_2} - \frac{1}{R_1} - \frac{1}{R_3}\right); \tag{3}$$

The pressure difference on the continuous and discrete phases can also be related by imposing that the total flow rate, the sum of the flow rates of both phases, through a cross-section away from the constriction must vanish:

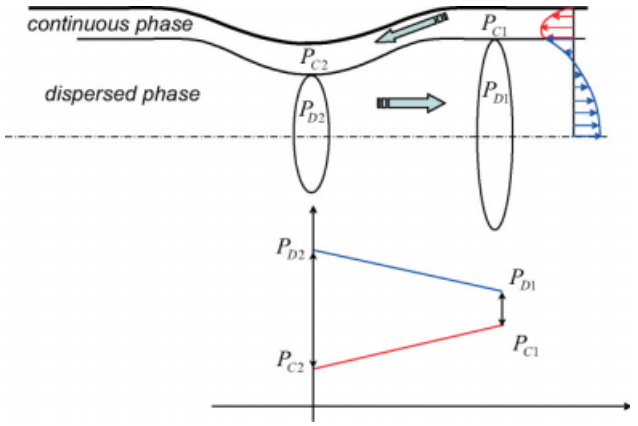

Figure 2. Sketch of pressure difference of both phases along the capillary axis and of the velocity profile away from the capillary throat.

[Color figure can be viewed in the online issue, which is available at www.interscience.wiley.com.]

$$\int_0^{R_1} r u_D(r)dr = \int_{R_1}^{R} r u_C(r)dr \approx \int_0^{\delta} R_1 u_C(y)dy \tag{4}$$

The velocity profile of the fully developed flow of both phases can be evaluated as a function of ΔP_D and ΔP_C by using the continuity of velocity and shear stress at the interface as boundary conditions for the momentum equation. Substituting the velocity profiles and the capillary pressure jump equation, Eq. 3, into Eq. 4, an expression for the pressure difference that drives the continuous phase towards the capillary throat can be derived:

$$\Delta P_C = \sigma\left(\frac{1}{R_2} - \frac{1}{R_1} - \frac{1}{R_3}\right)\frac{-\frac{R_1^3}{16\mu_D} - \frac{R_1^2\delta}{4\mu_C} + \frac{R_1\delta^2}{4\mu_C}}{-\frac{R_1^3}{16\mu_D} - \frac{R_1^2\delta}{4\mu_C} + \frac{\delta^3}{3\mu_C}}. \tag{5}$$

In this expression, δ is the thickness of the continuous phase film attached to the capillary wall. We assume it is always small, when compared with the capillary radius.

An assumption in this simple model is that the values of capillary pressure correspond to equilibrium conditions and that the drop is not moving through the capillary (static case). Figure 3 (top) shows the velocity profile of the continuous and dispersed phase at $R_1 = 48$ μm, $R_2 = 10$ μm, $\sigma = 5$ dyn/cm, $\delta = 2$ μm for a range of viscosity ratio $\kappa = \mu_D/\mu_C$. The continuous phase is assumed to be water, that is, $\mu_C = 1$ cP. The flow rate of the continuous phase towards the constriction falls as the viscosity of the dispersed phase rises. The main reason is that the shear stress at the interface that resists the flow of the continuous phase rises with the viscosity ratio. The velocity profile near the interface, presented in Figure 3b, shows how the velocity gradient at the interface of the continuous phase increases as the viscosity ratio becomes higher.

The snap-off time and the break-up of the drop are directly related to the flow rate of the continuous phase. The former can be evaluated by integrating the computed velocity profile. The effect of the viscosity ratio, $\kappa \equiv \mu_D/\mu_C$, on the dimensionless flow rate defined as $Q/[(\sigma/\mu)A]$ at the

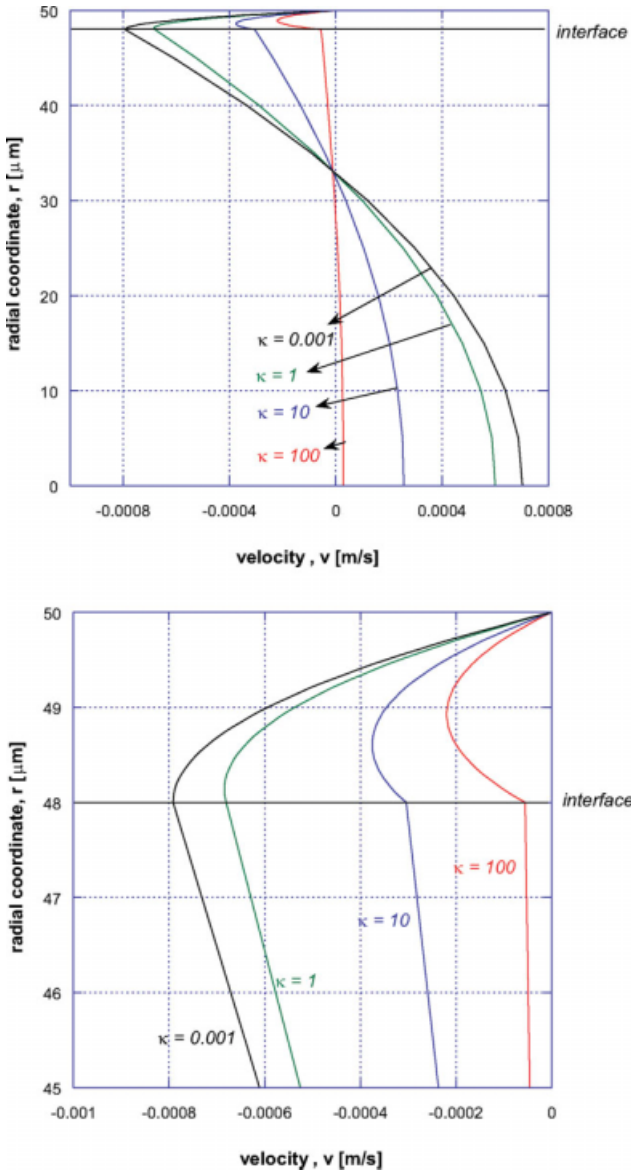

Figure 3. Velocity profile of the continuous and discrete phase as a function of the viscosity ratio κ.

[Color figure can be viewed in the online issue, which is available at www.interscience.wiley.com.]

same geometric parameters used in Fig.3 is presented in Figure 4. As expected, at a fixed viscosity ratio, the flow rate in the continuous phase rises with the interfacial tension σ, because the capillary pressure difference is the driving force of the flow. At each value of interfacial tension, the flow rate does not vary appreciably with the dispersed phase viscosity for viscosity ratio less than $\kappa = 1$. However, it drops significantly as the viscosity ratio becomes larger than 1. At higher viscosity ratio, the shear stress at the interface cannot be neglected and the flow rate becomes very small, which may explain why snap-off may not occur if the drop viscosity is much larger than the continuous phase viscosity.

The experiments presented next agree with this simple theoretical model: snap-off was not observed when the viscosity ratio was larger than $\kappa \approx 100$.

Experimental Setup

Different emulsions were prepared to study the effect of the viscosity ratio of the two phases on the snap-off mechanism. Different mineral oils and pure *n*-heptane were used as dispersed phase; water (pure or with surfactant) and glycerin-water solutions were used as continuous phase to cover a wide range of viscosity ratio. Table 1 shows the eight different systems used in the experiments, listing the disperse and continuous phase, the viscosity ratio, and the interfacial tension for each emulsion. The viscosity of each component was measured using a Cannon-Fenske viscosimeter and the interfacial tension was obtained by the ring method. The surfactant, when used, was Sodium Dodecyl Sulfate (SDS) at a concentration of 0.03 M (×3 CMC). Because of the low values of Bond number, the density ratio between the liquids does not affect the experiments and were not considered in this analysis. Both liquid phases were gently mixed to produce emulsions with large drops (>1 mm).

The experimental apparatus used is shown in Figure 5. A syringe pump was used to feed the emulsions with large drops, much larger than the constriction radius, through the constricted capillary at a constant volumetric flow rate. Related work of cross-flow drop generation (T-junction generators) show that large drops always break.[5] A borosilicate glass capillary was used to simulate a pore passage of a porous media, as shown at the bottom of Figure 5. The pore body-pore throat systems is defined by the capillary diameter

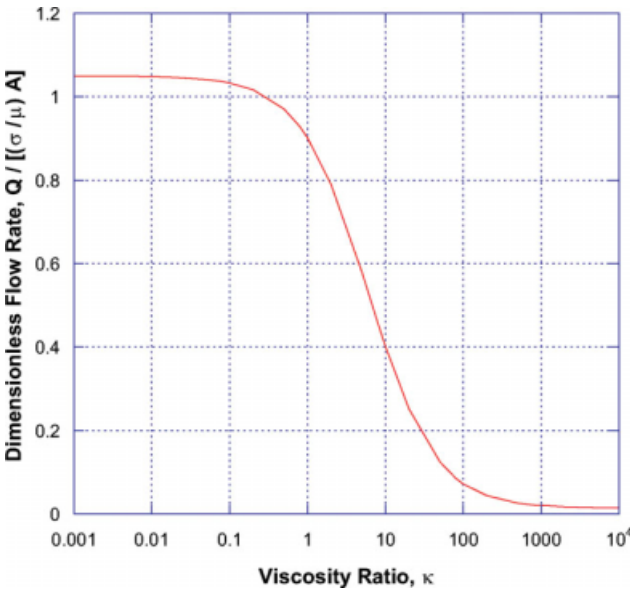

Figure 4. Dimensionless flow rate of the continuous phase towards the capillary throat as a function of the viscosity ratio and interfacial tension σ.

[Color figure can be viewed in the online issue, which is available at www.interscience.wiley.com.]

Table 1. Liquid Systems Used in the Experiments

Liquid System	Continuous Phase	Dispersed Phase	Viscosity Ratio κ	Interfacial Tension σ [mN/m]
1	*n*-heptane	Glycerin/water sol. 55%	0.056	21.7
2	*n*-heptane	Glycerin/water sol. 40%	0.124	25.5
3	*n*-heptane	SDS water solution	0.4	17.2
4	SDS water sol.	OP3	3.5	9.8
5	SDS water sol.	OP10	13.4	6.7
6	SDS water sol.	OP35	57	6.7
7	SDS water sol.	Talpa 30	460	5.3
8	Water	Talpa 30	460	17.9

$D_T = 200\ \mu$m and the constriction diameter $D_C = 50\ \mu$m. The radius of the transversal curvature of the throat R_3, which was much larger than the other two radii was neglected in the analysis. The capillary tube was mounted on a Axiovert 40 MAT inverted microscope (from Carl Zeiss). The tubing connecting the syringe to the capillary was made as short and as rigid as possible to minimize the expansion of the tubing as the inlet pressure rises during the experiments. Images of the flow were captured by a CCD camera attached to the microscope and connected directly to the frame grabber and then recorded on a video tape. The capturing rate of the camera was set to 15 frames per second. An 10× objective was used to observe details of the snap-off process, whereas objectives of 2.5× and 5× were used to gather a wider field of view of the constriction. Undesirable refractive index contrasts were mitigated by submerging the capillary in a small container filled with glycerin.

For each emulsion, the flow rate was slowly raised from 0.01 ml/h to 0.2 ml/h, which corresponded to an average fluid velocity in the straight section of the capillary varying $V = 8.8 \times 10^{-5}$ to 1.8×10^{-3} m/s and a capillary number range of $Ca = 4.1 \times 10^{-6}$ to 5.8×10^{-4}. At each flow rate, the passage of large drops through the constriction was observed to determine the conditions that lead to drop breakup. These conditions were mapped in the parameter space as a function of the capillary number Ca and viscosity ratio between the dispersed and continuous phases, κ, defined as

$$Ca \equiv \frac{\mu_C V}{\sigma}; \tag{6}$$

$$\kappa \equiv \frac{\mu_D}{\mu_C}. \tag{7}$$

μ_C and μ_D are the viscosities of the continuous and dispersed phases, σ is the interfacial tension, and V is the average velocity of the flow in the straight section of the capillary.

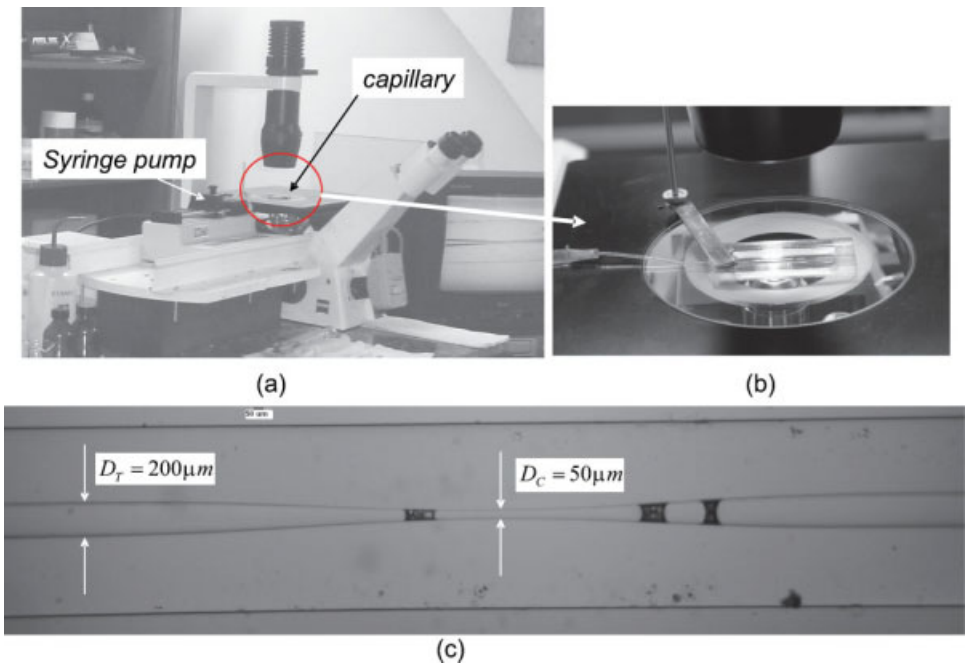

Figure 5. Sketch of the experimental setup, showing the syringe pump, microscope and constricted capillary.

Geometry of the capillary near the throat is show at the bottom of the figure. [Color figure can be viewed in the online issue, which is available at www.interscience.wiley.com.]

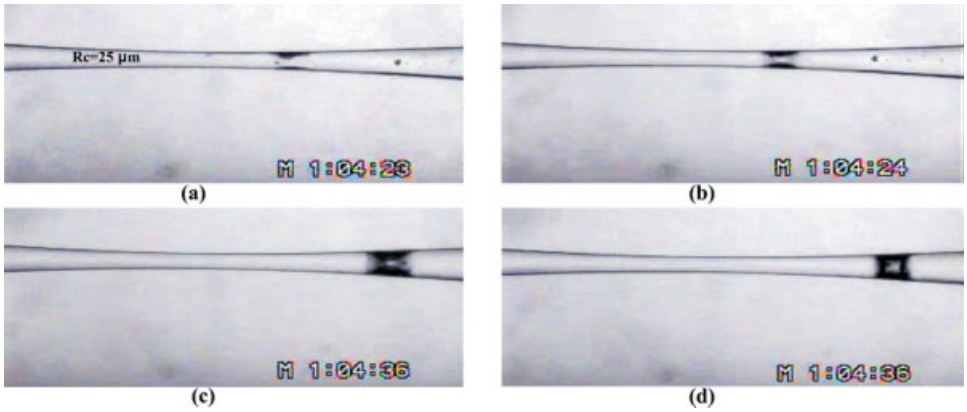

Figure 6. Evolution of the collar structure of the continuous phase until snap-off.

[Color figure can be viewed in the online issue, which is available at www.interscience.wiley.com.]

Results

As a drop flows through the straight portion of the capillary, a thin film of the continuous phase is left attached to the capillary wall. The thickness of this film is proportional to the capillary number raised to 2/3.[21] At low capillary number, the continuous phase film thickness is very small. At $D_T = 200$ μm and $Ca = 10^{-3}$, it is approximately $h_c \approx 1$ μm. Typically the capillary number for microfluidic droplet formation ranges from $Ca \sim 10^{-3}$ to 10^{1}.[4]

As discussed before, a capillary pressure gradient along the thin film attached to the wall is created due to the higher curvature of the drop interface near the constriction. This pressure difference drives a flow of the continuous phase toward the constriction. The accumulation of the continuous phase leads to a collar structure that grows until the drop breaks up. An example of this sequence is depicted in Figure 6 for liquid system 4 (viscosity ratio $\kappa = 3.5$). The drop flows from left to right in the figure and the capillary number was approximately $Ca \approx 10^{-5}$. The initial stages of the collar formation are shown in Figure 6a. The growth of the collar and the choking process of the oil drop is clear in Figures 6b, c. In the last frame (d), the large drop breaks into two smaller drops. In these images, the continuous phase (water) was dyed with a dark color to improve the contrast between the two phases.

The region of the parameter space, defined by the capillary number and viscosity ratio, at which the snap-off occurred is presented in Figure 7. The open symbols in the plot indicate experimental conditions at which drop break up was not observed. Filled symbols indicate conditions at which snap-off occurred. At a viscosity ratio $\kappa \equiv \mu_D/\mu_C = 0.056$, the large drop broke for the entire range of capillary number explored, from $7 \times 10^{-5} < Ca < 7 \times 10^{-4}$ (this is much lower than typical capillary number windows in microfluidics applications[4]). This observation agrees with the results of Gauglitz et al.,[18] who were able to measure a finite snap-off time of gas bubbles ($\kappa \to 0$) for the entire range of capillary number they explored ($10^{-5} < Ca < 10^{-2}$). At higher viscosity ratio, $\kappa \geq 57$, snap-off was not observed for the entire range of capillary number explored. This observation agrees with the simple model described in the previous section. For viscosity ratios in the range $0.124 \leq \kappa \leq 13.36$, there was always a capillary number above which the (infinite) drop would flow through the capillary throat without breaking.

It is important to note here that the upper limit on the range of capillary number at which snap-off of a gas bubble occurs reported by Tsai and Miksis[15] was related to the falling residence time of the bubble with rising capillary number. Our drops were considered to be infinite, because the residence time of each one at the conditions at which snap-off was not observed was larger than 10 min. Although not unambiguously conclusive, our results suggest that the upper limit on the range of capillary number is not related to the short residence time of the drop in the constriction. There is a possibility related to much larger time scale for snap-off than allowed by our experimental conditions. In principle, the inhibition of snap-off appears to be against the observations reported in the literature for gas bubbles flowing

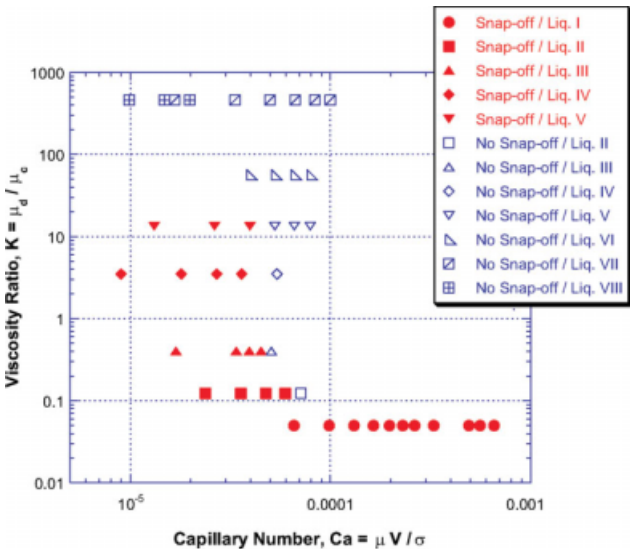

Figure 7. Map of the operating conditions at which snap-off was observed.

Open symbols represent conditions at which snap-off did not occur. [Color figure can be viewed in the online issue, which is available at www.interscience.wiley.com.]

through constrictions. Gauglitz et al.[18] reports that the snap-off time falls with capillary number. The reason is that the thickness of film attached to the capillary wall rises with capillary number and consequently the flow resistance falls. On the other hand, in flows at high capillary number, the surface tension driven forces are weaker than viscous forces. In the limit at $Ca \rightarrow \infty$, $\frac{\sigma}{V\mu_c} \rightarrow 0$ and the driving force for snap-off vanishes. In this limiting case, it is expected that snap-off will not occur. Consequently, there should be a finite critical value of capillary number above which the viscous stress at the wall is stronger than the capillary driven flow and snap-off is not observed.

Final Remarks

Visualization experiments of oil-water emulsions flow through a constricted capillary were successfully carried out with the objective of analyzing the parametric behavior of the snap-off process as a function of oil-water viscosity ratio and capillary number.

At intermediate viscosity ratio, the region in the parameter space at which drop snap-off occurs is bounded by a critical capillary number above which the drop flows through the neck without breaking. This critical capillary number values appears to be a decreasing function of the oil-water viscosity ratio. The results show that if the viscosity of the dispersed phase is high enough, the mechanism is suppressed.

Most systems analyzed in recent times involve gas as the dispersed phase. In this particular case, the dispersed-phase viscosity can be neglected. Our results indicate that oil viscosity is relevant to analyze the competing forces in the snap-off process. In this sense, a mechanistic model has been proposed, which is consistent with our experimental results.

Additional geometries of the capillary tube will be assessed in future work. This includes different curvatures of the cylindrical capillary tubes with a constriction and square cross-sectional area of the neck.

Acknowledgments

This work was funded by CNPq (Brazilian Research Council) and Petrobras.

Literature Cited

1. Nakashima T, Shimizu M, Kukizaki M. Particle control of emulsion by membrane emulsification and its applications. *Adv Drug Deliv Rev*. 2000;45:47–56.
2. Nisisako T, Okushima S, Torii T. Controlled formulation of monodisperse double emulsions in a multiple-phase microfluidic system. *Soft Matter*. 2005;1:23–27.
3. van der Graaf S, Schroën CGPH, van der Sman RGM, Boom RM. Influence of dynamic interfacial tension on droplet formation during membrane emulsification. *J Colloid Interface Sci*. 2004;277:456–463.
4. Christopher GF. Microfluidic methods for generating continuous droplet streams. *J Phys D: Appl Phys*. 2007;40:R319–R336.
5. Link DR, Anna SL, Weitz DA, Stone HA. Geometrically mediated breakup of drops in microfluidic devices. *Phys Rev Lett*. 2004;92:054503–1–054503–4.
6. Teh S-Y, Lin R, Hung L-H, Lee AP. Droplet microfluidics. *Lab Chip*. 2008;8:198–220.
7. Li W, Young WK, Seo M, Nie Z, Gartecki P, Simmons CA, Kumacheva E. Simultaneous generation of droplets with different dimensions in parallel integrated microfluidic droplet generators. *Soft Matter*. 2008;4:258–262.
8. Davies GA, Nilsen FP, Gramme PE. The formation of stable dispersions of crude oil and produced water: the influence of oil type, wax and asphaltene content. Paper SPE 36587 presented at: SPE Annual Technical Conference and Exhibition, October 1996, Denver, Colorado.
9. Sarbar MA, Wingrove MD. Physical and chemical characterization of Saudi Arabian crude oil emulsions, paper SPE 38817, 1997:675–685.
10. Kokal S. Crude-oil emulsions: a state-of-the-art review. *SPE Prod Facilities*. 2005;20:5–13.
11. Jensen PH. Characterization of oil-water mixtures produced in high-watercut oil wells, PhD Thesis, Delft University of Technology, 2000.
12. Roof JG. Snap-off of oil droplets in water-wet pores. *SPE J*. 1970;10:85–90.
13. Olbricht WL, Leal LG. The creeping motion of immiscible drops through a converging/diverging tube. *J Fluid Mech*. 1983;134:329–355.
14. Aul RW, Olbricht WL. Stability of a thin annular film in pressure-driven, low-Reynolds-number flow through a capillary. *J Fluid Mech*. 1990;215:585–599.
15. Tsai TM, Miksis MJ. Dynamics of a drop in a constricted capillary tube. *J Fluid Mech*. 1994;274:197–217.
16. Arriola A, Willhite GP, Green DW. Trapping of oil drops in a noncircular pore throat and mobilization upon contact with a surfactant. *SPE J*. 1983;23:99–114.
17. Ratulowski J, Chang HC. Snap off at strong constrictions - effect of pore geometry. *ACS Symp Series*. 1988;373:282–294.
18. Gauglitz PA, St. Laurent CM, Radke CJ. Experimental determination of gas-bubble breakup in a constricted cylindrical capillary. *Ind Eng Chem Res*. 1988;27:1282–1291.
19. Gauglitz PA, Radke CJ. The dynamics of liquid film breakup in constricted cylindrical capillaries. *J Colloid Interface Sci*. 1990;134:14–40.
20. Olbricht WL. Pore-scale prototypes of multiphase flow in porous media. *Annu Rev Fluid Mech*. 1996;28:187–213.
21. Bretherton FP. The motion of long bubbles in tubes. *J Fluid Mech*. 1961;10:166–188.

Manuscript received Apr. 2, 2008, revision received Nov. 11, 2008, and final revision received Jan. 10, 2009.